The Effect of Branch Angle on Human Coronary Artery Blood Flow

Peter R. Johnston and David Kilpatrick
University of Tasmania, Hobart, Australia

Abstract Despite its prevalence, little is known about the initiating factors for coronary artery disease. Some researchers believe that regions of low wall shear stress predispose to atheroma and subsequent narrowing, while others believe that narrowing is initiated by high shear stress. This paper presents steady state and transient three dimensional modelling studies of blood flowing through the left main stem, left anterior descending (LAD) and left circumflex coronary arteries (LCX), where the angle at which the LAD leaves the left main stem was varied through an angle of 90°. The Reynolds number for steady flow was 205 and for transient flow it was 216 (at peak velocity) with the LCX to LAD flow ratio being 9:11 in both cases. Further, the transient simulations included a period of reversed flow corresponding to contraction of the heart. Steady state simulations showed a region of high wall shear stress on the downstream side of the LCX as well as another region slightly upstream from the junction in the left main stem. The transient simulations, representing phasic flow, showed that there was a change in position of the extremes in the wall shear stress throughout the cardiac cycle. Changing the branch angle changed the position of the extremes in the wall shear stress distribution. With an acute angle between the left main stem and the LAD, high wall shear stress was observed downstream from the artery junction with low wall shear stress observed almost on the point of the junction. With an obtuse angle, the region of low wall shear stress was widely spread on the upstream side with a concentrated region of high wall shear stress near the junction on the downstream side. These simulations show that the initiating factors for arterial narrowing vary through the cardiac cycle and depend on branch angle.

1. INTRODUCTION

Coronary artery disease is one of the major causes of death in western society and at present its initiating factors are still unknown. Some authors believe it is due to high wall shear stress (Fry, 1968), but others believe it is due to low wall shear stress (Caro et al., 1971). This paper presents a modelling study of the fluid mechanics of blood flow in a bifurcation of a coronary artery with a view to predicting regions of high and low wall shear stress. In particular, changes in the wall shear stress distribution due to various branch angles at the bifurcation will be considered. The ultimate aim is to correlate these regions with areas of arterial narrowing to provide an answer to the question of whether arterial geometry is associated with subsequent arterial stenosis.

1.1 Background

Fatty streaks occurring in the arterial wall have been shown (Stary, 1989) to lead to the true atheromatous plaques that form coronary artery disease. These streaks are known to be preferentially distributed at certain sites on the arterial walls. In particular these are the outer walls of arterial junctions and the inside of walls of curves. The non–uniform distribution of the fatty streaks suggests a position dependent wall permeability, enabling transport of cholesterol bearing lipoproteins in and out of the wall.

It has been shown that (Fry, 1968) if the arterial wall is subjected to (unphysiologically) high wall shear stress for a short period of time, the lining of the artery is irreversibly damaged and its permeability increases. This leads to the conclusion that high shear damage might be an initiating factor in coronary artery disease. Alternatively, it has also been shown (Caro et al., 1971) that fatty streaks develop in regions where low wall shear stress would be expected, given steady flow. This is consistent with the hypothesis that fatty streaks and early atheromatous plaques occur in regions of low wall shear stress.

A resolution to the shear stress question has been attempted experimentally (Asakura and Karino, 1990). Flow patterns in arteries from postmortem hearts, rendered transparent with ethanol and oil of wintergreen, were recorded by tracking polystyrene microspheres (in a suspension of oil of wintergreen and 5% ethanol) with 16–mm cine camera. Five different coronary artery trees were obtained, all from people whose primary cause of death was not cardiovascular disease, and the geometric integrity of the coronary trees was maintained by fixing them to a wire frame. The conclusion reached was that regions of slow or disturbed flow were associated with sites of narrowing.

Modelling blood flow in artery bifurcations using techniques of computational fluid dynamics is not new, but most attention has been directed to the flow through the carotid artery bifurcation (in the neck) (Rindt et al., 1990; Perktold and Resch, 1990; Perktold et al., 1991b; Rappitsch et al., 1993). These studies predict regions of flow separation and regions of high and low shear stress. They conclude that observed regions of low shear stress correlate with surgical findings on the location of narrowings. One recent study has looked at blood flow in the a single coronary artery containing only a slight

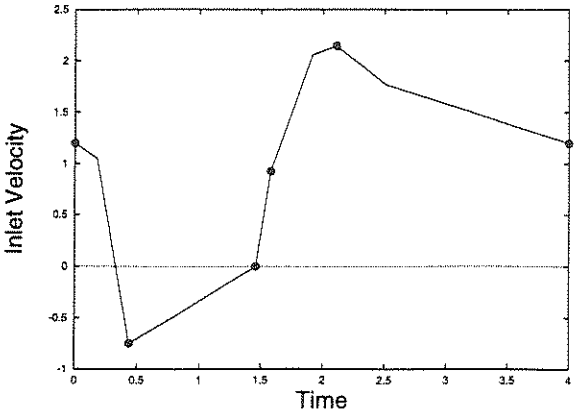

Figure 1: Flow Function for Fluid in the Left Main Stem

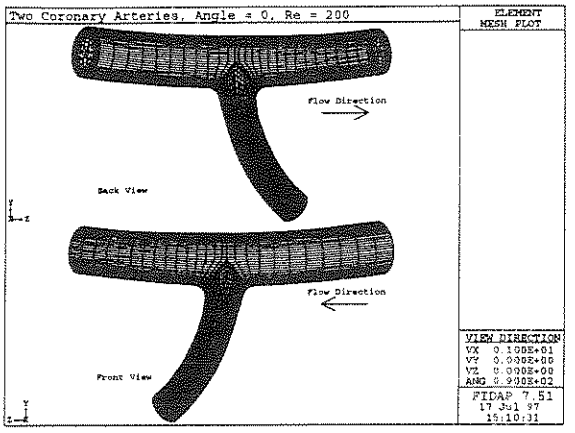

Figure 2: Finite Element Mesh for the Arterial Junction

curve and taper (Perktold et al., 1991a). From this study the importance of the secondary flows in the artery was emphasised, along with their relation to the wall shear stress and subsequent narrowing.

The junction considered here is that of the left main stem, left circumflex (LCX) and left anterior descending (LAD) arteries and this was chosen because of the high degree of arterial narrowing observed in the vicinity. This junction has been considered previously (Johnston and Kilpatrick, 1993) but there only a single branch angle was used; here, the effect of changing this branch angle is being considered.

2. SIMULATION

2.1 Governing Equations

Blood flow through the coronary arteries is assumed to be governed by the Navier–Stokes and continuity equations. The fluid is considered incompressible and the modelling is performed both transiently and at steady state. In rectangular coordinates the dimensionless governing equations are given by:

$$\frac{\partial \mathbf{v}}{\partial t} + \mathbf{v} \cdot \nabla \mathbf{v} = \frac{1}{Re} \nabla^2 \mathbf{v} - \nabla p \qquad (1)$$

and

$$\nabla \cdot \mathbf{v} = 0 \qquad (2)$$

where $\mathbf{v}$ is the velocity vector, p the pressure, t time and Re the Reynolds number. The equations have been rendered dimensionless with respect to D, the arterial diameter at the entrance and U, the maximum inlet velocity, also at the entrance. Hence the Reynolds number is given by $Re = \frac{\rho DU}{\mu}$, where ρ is the density of blood and μ the blood viscosity, assumed constant.

2.2 Boundary Conditions

The boundary conditions are such that there is no flow along the solid walls of the artery (no–slip condition). At the inlet, the fluid is assumed to have a fully developed Hagen–Poiseuille paraboloidal flow field. For the steady state problem this profile is assumed constant, whereas for the transient problem the magnitude of the centerline velocity is scaled according to the flow function in Figure 1 (Perktold et al., 1991a), whilst maintaining the paraboloidal field.

There are two outflow boundaries for this problem. At the first, the LCX artery, the flow is again assumed to have a paraboloidal velocity field, scaled, at any time, to be half of the inlet velocity, resulting in a 45%–55% flow divide between it and the LAD. At the second outflow boundary (on the LAD), stress free boundary conditions are applied and the pressure is set to zero for reference.

2.3 Solution Method

The governing equations are solved using the commercially available computational fluid dynamics package, FIDAP, based on the Galerkin finite element method (Engelman, 1982; Engelman, 1990). The equations are discretised on a non–uniform grid of approximately 13000 linear brick elements (Figure 2). Most of the elements are concentrated around the bifurcation point, increasing in size away from the junction. Elements are also concentrated near the walls of the arteries. A system of algebraic equations is obtained, from the mesh points and element connectivity, by integrating the shape functions from the Galerkin weighted residual representation of the governing equations. The pressure degree of freedom has been eliminated using a penalty function formulation (parameter, $\epsilon = 1 \times 10^{-6}$) and is recovered after the velocities have been calculated, thus reducing the size of the system of equations. A segregated solver, based on the conjugate gradient method, then solves the system of equations iteratively. The transient problem is solved using an implicit backward Euler time integration with variable time steps. At each time step a nonlinear system of equations is solved via the method described above.

2.4 Modelling Assumptions

There are two important assumptions in the model described above. The first is that blood is a Newtonian fluid. Blood can be considered to be a Newtonian fluid

only at high shear rates, because, at low shear, the shear rate – shear stress relationship curves towards the origin. The use of the Newtonian model is justified by the presence of high shear stresses in the modelling situation. Clearly, incorporating a non–Newtonian model would be an improvement. Secondly, the assumption of rigid arterial walls is justified by observing that most of the flow occurs during diastole when the heart is relaxed and the arteries are not subjected to external pressures. Also, the coronary arteries are the least elastic arteries in the body (Fischer and Llaurado, 1966) and so changes in dimension are small during the cardiac cycle.

2.5 Mesh Construction

The coronary artery junction was constructed from two mutually perpendicular angiograms. Each angiogram of the arterial tree was digitised and the pairs of points matched in three dimensional space, thus providing the centreline of the arterial junction. The full three dimensional structure was reconstructed using an in–house meshing programme which has the ability to alter many physical aspects of the arterial junction. This software allows the branch angle to be varied from its initial position whilst maintaining continuous curvature around the junction. It is necessary to maintain the curvature as the junctions in real arteries are smooth, unlike the intersection of two pipes.

For the simulations to be presented here, the branch angle was varied from its original position (denoted by angle = 0) (Figure 2) through an angle of 0.7 radians towards the LCX (angle = 7) and also through an angle of 0.8 radians towards the left main stem (angle = -8). These rotations give rise to a complete angular variation of approximately one right angle.

2.6 Wall Shear Stress

The most important quantity to be derived from the analysis is the wall shear stress. For incompressible fluids and no–slip conditions at the rigid wall, the dimensionless wall shear stress is

$$\tau_w = \frac{1}{Re} \left. \frac{\partial \mathbf{v}_t}{\partial n} \right|_{wall} \qquad (3)$$

where $\partial \mathbf{v}_t / \partial n$ is the partial derivative of the tangential velocity in the normal direction at the wall.

3. RESULTS

3.1 Steady Simulations

As described above, the angle between the LAD and left main stem was varied through approximately one right angle. Steady state flow simulations were performed at 0.1 radian intervals from -0.8 radians from the initial position, through the initial position to 0.7 radians in the other direction. Figure 3 shows the wall shear distributions at branch angles of -0.6 (top), -0.2, 0.2 and 0.6 radians (bottom) from the initial position.

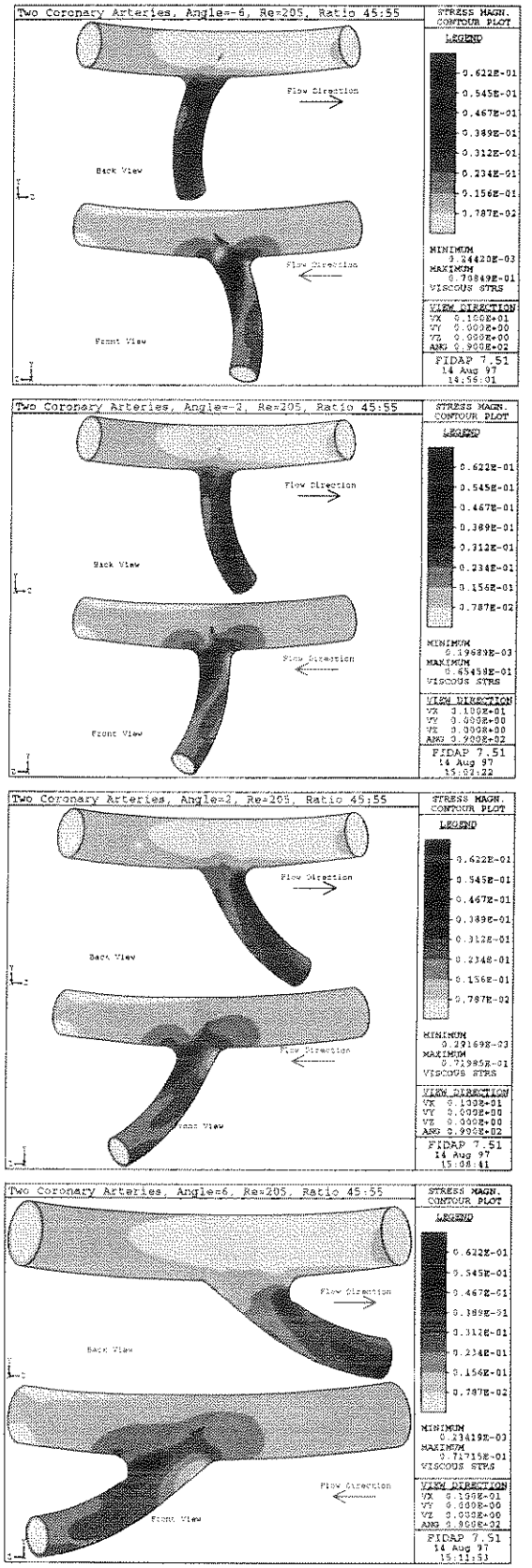

Figure 3: Wall Shear Stress Distributions at Various Branch Angles

Each subfigure shows a front and back view of the arterial junction. For the front view (lower image) the left

main stem/LCX artery is bowed out of the page and the LAD bends further out of the page as it leaves the junction. In the back view, the ends of the left main stem and LCX are bending back out of the page, while the LAD is bending back into the page.

Each distribution shows a region of high wall shear stress (dark area) on the downstream side of the LAD as well as a region of low wall shear stress (light area) on the upstream side. There is also a region of low wall shear stress at the back of the main artery above the junction.

One observation that can be made from the distributions is that as the angle between the left main stem and the LAD becomes less acute and then obtuse (moving from top to bottom in Figure 3), the regions of high and low wall shear stress move towards the junction on their respective sides of the LAD. Also, the region of high wall shear stress becomes more focussed, whereas the region of low wall shear stress remains constant in size.

Another thing to observe is that in the extreme cases of the obtuse angle, there is a very large gradient of wall shear stress on the downstream side of the LAD. This arises due to the close proximity of the point of high wall shear stress to a small region of low wall shear stress visible on the back view of the bottom panel of Figure 3.

3.2 Transient Simulations

Figures 4, 5 and 6 show distributions of wall shear stress at various points of the cardiac cycle for the original (Figure 5) bifurcation angle and the extreme angles considered (Figures 4 and 6). The points in the cardiac cycle chosen for display are shown as dots in Figure 1 with the exception of the point where the inlet velocity is zero. At that point the wall shear stress is low (on the scale chosen for plotting) all through the junction. The other points chosen are at the start of the cycle (top panel), just before the flow begins rapid deceleration ($t = 0.0$), at the point of maximum reverse flow ($t = 0.456$), the point of maximum acceleration of the blood ($t = 1.576$) and the point of maximum forward flow ($t = 2.108$) (bottom panel). Clearly the point at the end of the cycle is the same as the first point.

Considering all three branch angles, it can be seen that the maximum shear stresses are very similar during the deceleration and reverse flow phases of the cardiac cycle. However, in the acceleration and forward flow phases, the obtuse angle geometry (Figure 6) produces higher maximum wall shear stress than the other two geometries considered. The behaviour of the minimum values of the wall shear stress is more difficult to describe, as is the range of wall shear stress values.

From Figures 4 and 5 it can be seen that a region of high wall shear stress appears on the upstream side of the LAD during flow reversal. However, this is not observed when the branch angle is obtuse (Figure 6). A possible explanation for this is the smooth way in which the LAD is joined onto the left main stem on the upstream side. Such a joint allows smooth merging of the blood in the LAD with that in the main artery without greatly impinging on artery wall.

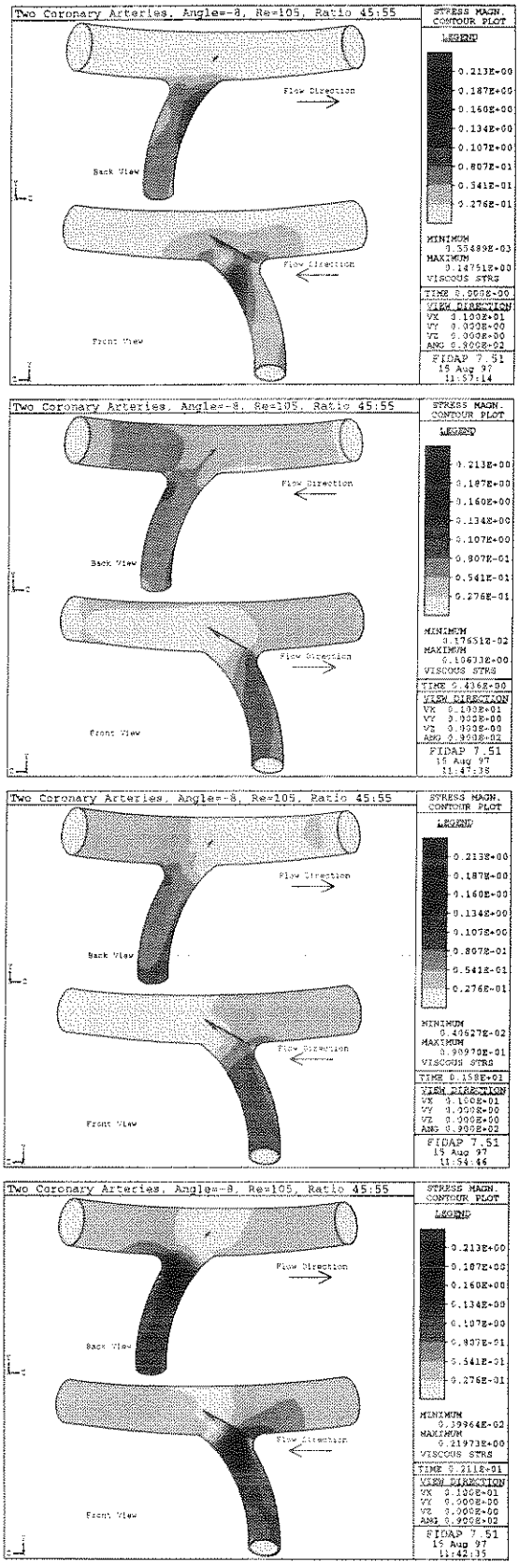

Figure 4: Transient Wall Shear Stress Distributions for angle = -8

As perhaps would be expected, the region of high wall shear stress becomes more focussed as the velocity of

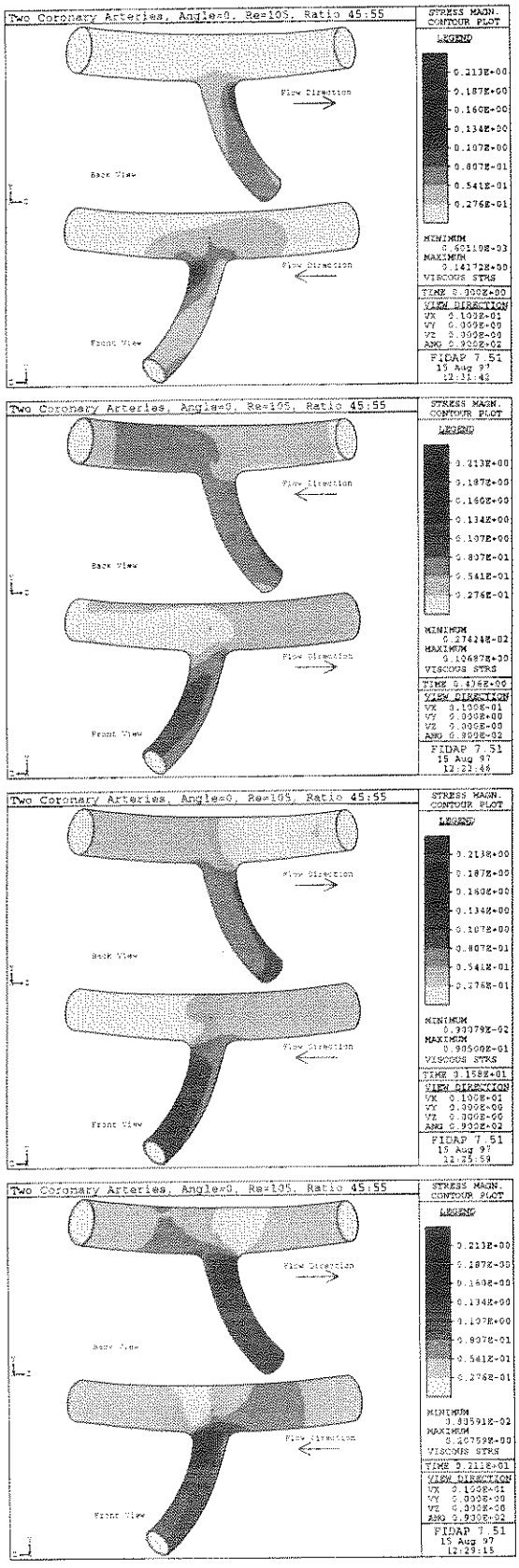

Figure 5: Transient Wall Shear Stress Distributions for angle = 0

the blood increases, especially in the forward direction. Also, as was observed in the steady state cases, the point of focus of the high wall shear stress moves towards the artery junction, on the downstream side of the LAD, as the bifurcation angle moves from acute to obtuse. This is also true for the regions of low wall shear stress on the upstream sides of the LAD.

Apart from considering the wall shear stress itself, another quantity of potential interest is the spatial gradient of wall shear stress. The gradient is only really large during the parts of the cycle for which the blood velocities are high. During the low flow rate periods the wall shear stress distribution is reasonably flat with the steepest gradients occurring in the case of the acute branch angle. During the high flow rate phases, the steepest gradients generally occur for the acute branch angle, but there is one region of very steep gradient on the back of the LAD on the downstream side in the obtuse angle case.

In most of the simulations considered, the wall shear stress on the inside curve of the main artery above the junction is reasonably low, and it remains that way during the cardiac cycle. Also, there are mainly low gradients of wall shear stress in this region.

4. CONCLUSIONS

From these simulations it can be seen that the distribution of wall shear stress along the walls of the coronary arteries during the cardiac cycle is very complex. It would appear that there is no simple relationship between the distribution of the wall shear stress and the flow conditions at the entrance to the computational domain. One general conclusion is that the extremes in wall shear stress change sides of the LAD during the reversed flow phase of the cardiac cycle. However, this is not observed at an obtuse angle between the LAD and the left main stem.

Clearly, there is a complex relationship between the wall shear stress and the sites of arterial narrowing. It is possible that arterial narrowing occurs in regions which are subject to low shear rates for "most" of the cardiac cycle. This in turn raises the question of whether temporal gradients of wall shear stress play a part in the initiation of coronary artery disease.

5. ACKNOWLEDGEMENTS

This work was funded, in part, by the Australian Research Council, the National Heart Foundation of Australia and the Royal Hobart Hospital Acute Care Programme.

6. REFERENCES

Asakura, T. and Karino, T. Flow patterns and spatial distribution of atherosclerotic lesions in human coronary arteries. *Circ. Res.*, 66:1054–1066 (1990).

Caro, C. G., Fitz-Gerald, J. M., and Schroter, R. C. Atheroma and arterial wall shear: observation, correlation and proposal of a shear dependent mass

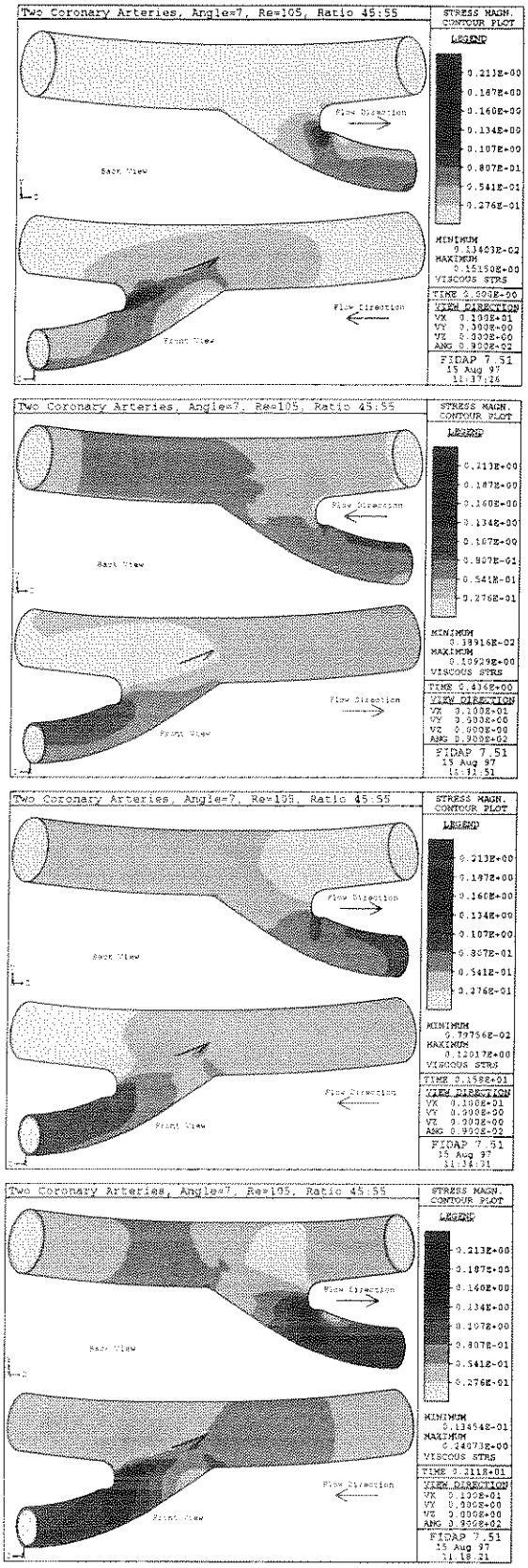

Figure 6: Transient Wall Shear Stress Distributions for angle = 7

transfer mechanism for atherogenesis. *Proc. R. Soc. Lond.*, B177:109–159 (1971).

Engelman, M. S. FIDAP – a fluid dynamics analysis package. *Adv. Engng Softw.*, 4:163–166 (1982).

Engelman, M. S. *FIDAP User's Guide*. Fluid Dynamics International, Evanston,Illinois, version 5.0 edition (1990).

Fischer, G. M. and Llaurado, J. G. Collagen and elastin content in canine arteries selected from functionally different vascular beds. *Circ. Res.*, 19:394–399 (1966).

Fry, D. Acute vascular endothelial changes associated with increased blood velocity gradients. *Circ. Res.*, 22:165–197 (1968).

Johnston, P. R. and Kilpatrick, D. A transient analysis of human coronary artery blood flow. In Held, K., Brebbia, C., Ciskowski, R., and Power, H., editors, *Computational Biomedicine*, pages 93–100, Bath, U.K. Computational Mechanics Publications (1993).

Perktold, K., Nerem, R. M., and Peter, R. O. A numerical calculation of flow in a curved tube model of the left main coronary artery. *J. Biomechanics*, 24(3–4):175–189 (1991a).

Perktold, K. and Resch, M. Numerical flow studies in human carotid artery bifurcations: basic discussion of the geometry factor in atherogenesis. *J. Biomed. Eng.*, 12:111–123 (1990).

Perktold, K., Resch, M., and Peter, R. O. Three–dimensional numerical analysis of the pulsatile flow and wall shear stress in the carotid artery bifurcation. *J. Biomechanics*, 24(6):409–420 (1991b).

Rappitsch, G., Perktold, K., and Guggenberger, W. Numerical analysis of intramural stresses and blood flow in arterial bifurcation models. In Held, K. D., Brebbia, C. A., Ciskowski, R. D., and Power, H., editors, *Computational Biomedicine*, pages 149–156, Bath, U.K. Computational Mechanics Publications (1993).

Rindt, C. C. M., van Steenhoven, A. A., Janssen, J. D., Reneman, R. S., and Segal, A. A numerical analysis of steady flow in a three–dimensional model of the carotid artery bifurcation. *J. Biomechanics*, 23(5):461–473 (1990).

Stary, H. C. Evolution and progression of atherosclerotic lesions in coronary arteries of children and young adults. *Arteriosclerosis*, 9(1):I–19 – I–32 (1989).